AD_____

Award Number: W81XWH-05-1-0108

TITLE: Non-Invasive Markers of Tumor Growth, Metastases, and Sensitivity to Anti-Neoplastic Therapy

PRINCIPAL INVESTIGATOR: Jason A. Koutcher

CONTRACTING ORGANIZATION: Sloan-Kettering Institute
New York, NY 10021

REPORT DATE: January 2008

TYPE OF REPORT: Annual

PREPARED FOR: U.S. Army Medical Research and Materiel Command
Fort Detrick, Maryland 21702-5012

REPORT DOCUMENTATION PAGE

Form Approved
OMB No. 0704-0188

1. REPORT DATE	2. REPORT TYPE	3. DATES COVERED
05-01-2008	Annual	6 DEC 2006 - 5 DEC 2008

4. TITLE AND SUBTITLE
Non-Invasive Markers of Tumor Growth, Metastases, and Sensitivity to Anti-Neoplastic Therapy

5a. CONTRACT NUMBER

5b. GRANT NUMBER
W81XWH-05-1-0108

5c. PROGRAM ELEMENT NUMBER

6. AUTHOR(S)
Jason A. Koutcher

Email: koutchej@mskcc.org

5d. PROJECT NUMBER

5e. TASK NUMBER

5f. WORK UNIT NUMBER

7. PERFORMING ORGANIZATION NAME(S) AND ADDRESS(ES)
Sloan-Kettering Institute
NY, NY 10021

8. PERFORMING ORGANIZATION REPORT NUMBER

9. SPONSORING / MONITORING AGENCY NAME(S) AND ADDRESS(ES)
U.S. Army Medical Research and Materiel Command
Fort Detrick, Maryland 21702-5012

10. SPONSOR/MONITOR'S ACRONYM(S)

11. SPONSOR/MONITOR'S REPORT NUMBER(S)

12. DISTRIBUTION / AVAILABILITY STATEMENT
Approved for Public Release; Distribution Unlimited

13. SUPPLEMENTARY NOTES

14. ABSTRACT

The goals of this application are to develop methods to non-invasively differentiate fast and slow growing prostate tumors and also develop methods to evaluate response to anti-angiogenic agents. Validation of the results will be based on tumor growth, metastases, and microvessel density measurement (antiangiogenic studies). To date, we have succeeded in demonstrating that the R3327AT rat prostate tumor which is relatively radiation resistant, has detectable lactate which is heterogeneously distributed once the tumor exceeds 600mm3. In contrast, the radiation sensitive, slow growing Dunning H does not have lactate that is detectable by NMR. DCE-MRI studies do not suggest differences between slow and fast growing rat prostate tumors.

15. SUBJECT TERMS
NMR, prostate cancer, lactate, vascular permeability

16. SECURITY CLASSIFICATION OF:			17. LIMITATION OF ABSTRACT	18. NUMBER OF PAGES	19a. NAME OF RESPONSIBLE PERSON
a. REPORT	b. ABSTRACT	c. THIS PAGE			19b. TELEPHONE NUMBER *(include area code)*
U	U	U	UU	16	USAMRMC

Table of Contents

Introduction

The primary goal of this study is to determine whether non-invasive magnetic resonance (MR) techniques can distinguish between slow and rapidly growing and metastatic prostate tumors. This is particularly important in prostate cancer where 30% of men over the age of 50 have prostate cancer at autopsy but only 10% of men develop prostate cancer. Reliable methods do not exist to determine which cancers are aggressive and need to be treated vs. patients who could undergo watchful waiting. A second goal is to determine if anti-angiogenesis agents can be used as chronic low toxicity therapy for "newly diagnosed" tumors and as adjuvant to "curative" therapies and if MR techniques can be used as an early or *a priori* marker of tumor response. We propose that non invasive measurements of tumor vascular volume, permeability, choline and lactate will predict tumor aggressiveness (growth rate, tendency to metastasize). The hypothesis is based on data which indicates that tumor growth rates and metastases are related to angiogenesis which can be detected by dynamic contrast enhanced magnetic resonance imaging (DCE-MRI).

In addition, we propose to determine whether chronic anti-angiogenic therapy can be used in small "newly diagnosed" tumors and as an adjuvant to radiation. It will also be determined whether MRSI and DCE-MRI can predict response to anti-angiogenic therapy. We will also study the effect of anti-angiogenic therapy in small "newly diagnosed" tumors and also as an adjuvant post radiation to determine if it delays tumor growth and metastases. Tumor doubling times and number of metastatic lesions in the lung will be the biological outcome measures. Developing chronic treatment modalities that delay (or obviate) the need for radical therapy will enhance treatment of prostate cancer and possibly quality of life. Similarly, developing a treatment that enhances response to radiation could potentially enhance the cure rate or delay recurrence which might alter subsequent therapy. The techniques applied here are available or readily implemented on clinical scanners (choline and lactate detection; DCE-MRI) so the research is highly translational.

Body

At the time of the previous report (9 months ago), we had finally succeeded in obtaining in vivo lactate measurements in tumor bearing rats. We had in essence lost a little more than 1 year in getting the tumors to grow and implementing 2 dimensional lactate imaging in vivo but those problems have been surmounted. Over the last year, we have made significant progress in acquiring the biological data proposed since in the previous year we had done all the technical work necessary.

Data Presentation: Biological

A. Data acquisition:

For MR studies, tumor bearing rats were anesthetized with isoflurane (1.0-2.5%) and compressed air. A 24 gauge tail vein catheter (Terumo Medical Corporation, Elkton, MD) was inserted into the tail vein prior to placing the tumor bearing rat in the magnet. MRS (magnetic resonance spectroscopy) lactate determination and dynamic contrast enhanced magnetic resonance studies were conducted for tumors in the range of 300-2860 mm3 in the Dunning H and 200-2860 in the Dunning R3327AT model. The studies were grouped based on similar tumor volumes for the data analysis. For the Dunning R3327-AT the groups were 200-400mm3, 700-850mm^3, 1400-1600 mm^3, 1850-2000 mm^3 and 2450-2850 mm^3. For the Dunning H models, the studies were grouped as 300-450mm^3, 650-800 mm^3, 1300-1650 mm^3, 1850-2250 mm^3 and 2425-2860 mm^3). Upon completion of the lactate studies, DCE-MRI (dynamic contrast enhanced magnetic resonance imaging) studies were performed on the rats without removing them from the magnet. Tumor bearing rats were typically studied 3 times. After the last study the tumor bearing rats were injected with pimonidazole (60mg/kg) and excised 60 minutes later. Pimonidazole and H&E staining were performed on tumor slices of 8 micron thickness.

MR experiments: MRS Experiments were performed on a Bruker 4.7 T, 40 cm bore animal scanner. A home-made 2 turn volume copper foil coil with a 25 mm diameter was used as a transmit-receive radiofrequency coil for all studies. Scout images were obtained in the three orthogonal directions to ensure that the tumor was positioned within the field of view. MRS lactate detection was performed using the selective multiple quantum coherence (Sel-MQC) (4) sequence, using selective 15 ms single-lobe Sinc pulses. The Sel-MQC sequence selectively detects lactate by selecting the zero quantum (ZQ) → double quantum (DQ) coherence transfer pathway. Phase cycling gradient combinations of g1:g2:g3 = 0:-1:2 with duration $\delta_1 = \delta_2 = 2$ ms, $\delta_3 = 4$ ms, and amplitude of 24 G/cm are used. The pulse sequence parameters for the lactate editing experiments included 512 data points, 8 averages, TR=2 s and a spectral width of 2500Hz. A matrix size of 16×16, FOV of 40 mm (2.5 x 2.5 mm in plane resolution) was used. Two-dimensional chemical shift imaging lactate maps were generated by selecting a 5 mm slice using a 1ms three-lobe Sinc pulse. The 2D CSI lactate map was visually coregistered with T2-weighted images of 5 mm slice thickness from the center of the tumor.

Upon completion of the lactate imaging, DCE-MRI studies were performed. Based on the previous scout images, 3 slices in the sagital direction were imaged using a gradient echo fast

imaging (GEFE) sequence with proton density weighted parameters. The acquisition parameters included 2 mm slice thickness, a gap of 0.2 mm, TR/TE/α = 500/3/30^o, 256 x 128 matrix, and 2 excitations per phase encoding step. Subsequently the dynamic images were obtained using the same parameters as above except that the TR was reduced to 50ms and 288 data sets were obtained. Gd-DTPA (0.2 mM/kg) was injected intravenously after the first 5 images of the dynamic train had been acquired and these images were used to measure the precontrast signal intensity under saturation conditions.

Data Processing: DCE-MRI data were analyzed using the two compartment model of Hoffman et al (1) to evaluate the rate constant "k_{ep}" and Ak_{ep} (A = amplitude – one of the parameters from the fitting of the data to the model; k_{ep} = rate constant for transfer of Gd-DTPA from the interstitial compartment to the plasma) and slope (rate of increase of signal/time) using IDL programs written previously for clinical studies. In addition the data are currently being analyzed using the model of Tofts (2). An arterial input function is being estimated from the DCE-MRI studies of 4 normal (non-tumor) bearing rats who underwent similar studies except that the abdomen was imaged using a whole body coil. This allows us to measure the changes in signal intensity in the aorta and abdominal vena cava and to derive an arterial input function. We have shown previously that using an averaged arterial input function instead of an individualized one leads to no systematic changes in K_{trans} (transfer constant) and v_e (interstitial volume) (3).

MRSI: Spatial Fourier transform and superimposition of the spectral grid on the corresponding T2-weighted image were performed using the 3DiCSI software package (courtesy of Truman Brown, Ph.D., Columbia University). The voxels within the tumor were then identified and the free induction decay (FID) from each tumor voxel was extracted as numerical text data. The data for each FID was input to the jMRUI software package and the lactate resonance was fit in the time domain using AMARES (Advanced Method for Accurate ,Robust, and Efficient Spectral fitting)(4). The reference phantom 2DCSI set was processed similarly. For quantitation purposes, each tumor voxel was referenced to a phantom voxel at the exact same location. The tumor voxel lactate peak area, the reference voxel lactate peak area, the appropriate T1 saturation factors and the comparative coil loading parameters for tumor and phantom studies and were then used to quantify the tumor voxel lactate.

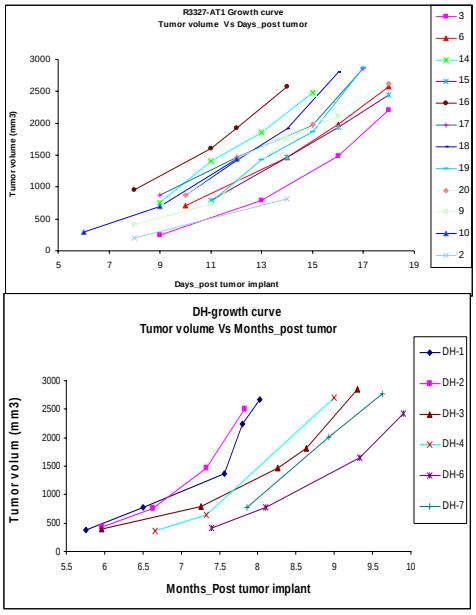

Fig. 1 Top: Growth Curve of Dunning R3327. Bottom: Growth Curve of Dunning H tumor. Note different x axes

D. Results

Figure 1 shows a growth curve for the Dunning R3327AT and Dunning H tumor. The differences in growth rate are readily apparent (note different scales on the x axis). Figure 2a shows a typical set of CSI spectra for a single Dunning R3327AT tumor as it grew in size from 618 to 2008 mm3. At all tumor volumes, lactate is readily

detected and it is noted to increase qualitatively as the tumor grew although at large tumor volumes (2008mm3) the signal to noise ratio has decreased suggesting a decrease in lactate

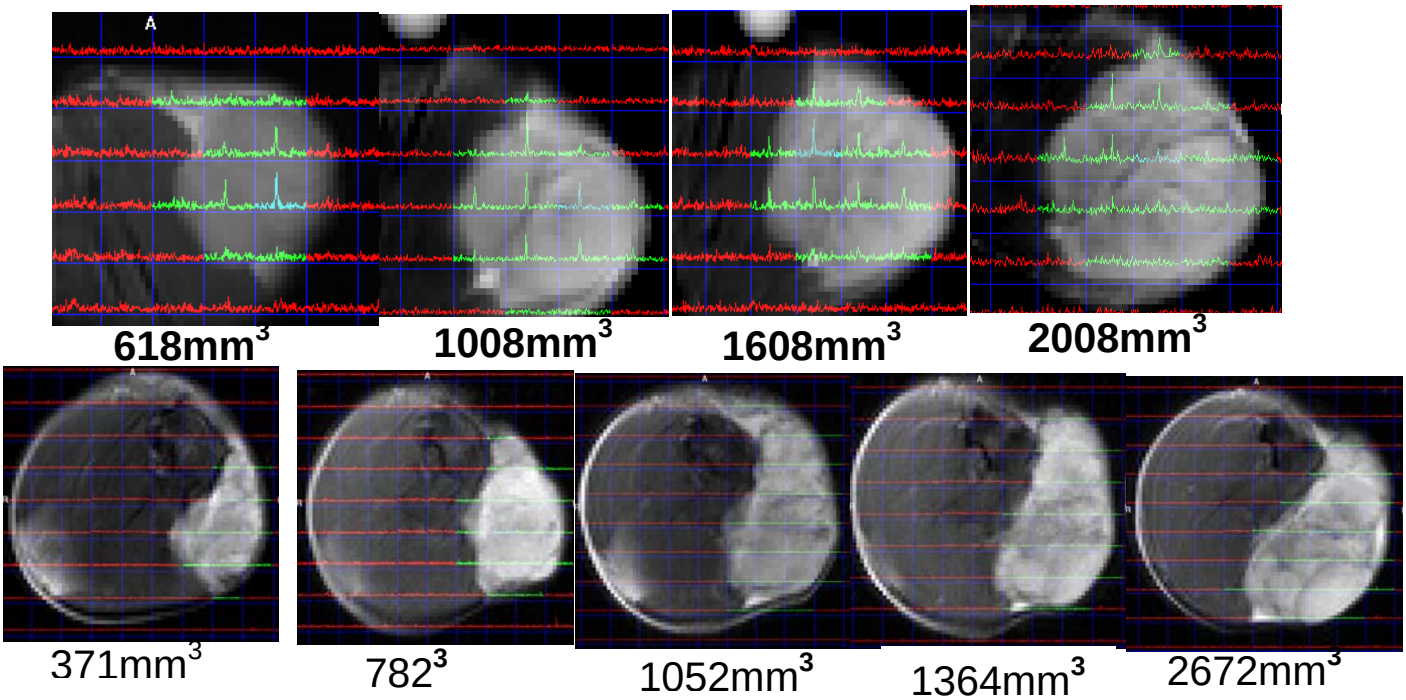

Fig. 2 Top. Chemical shift image (CSI) of Dunning R3327AT tumor with growth. Lactate is detected when the tumor is about 600mm3 (at smaller tumor volumes lactate was not seen) and increases with tumor growth but decreases as the tumor gets very large and probably necrotic. Bottom: CSI from Dunning H tumor – no lactate was detected.

concentration. In contrast, Fig. 2b shows similar data obtained on the Dunning H wherein lactate cannot be detected independent of tumor volume.

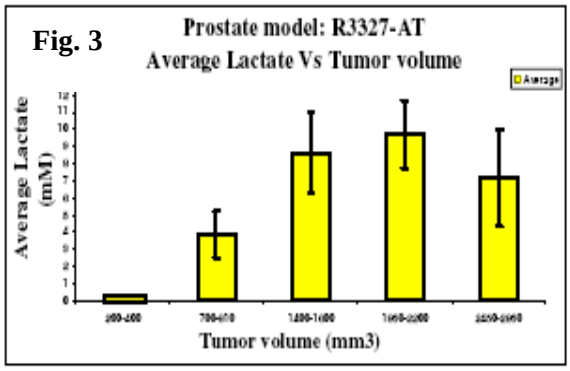

Fig. 3. Average concentration of lactate and how it changes with tumor growth. At volume below 400mm3, no lactate was shown and the small yellow bar is placed to indicate that a measurement was done.

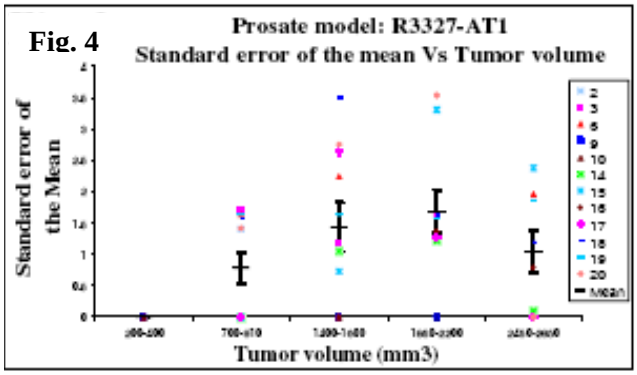

Fig. 4. Average standard error of the mean (SEM)for lactate/voxel. The SEM values were averaged for each volume range to provide an estimate of heterogeneity of lactate in the tumor in the different size ranges.

Figure 3 shows the average amount of lactate present in the R3327AT tumor and how it varies with tumor growth. Lactate is not detected at small tumor volumes in the 3 tumors between 200 and 400 mm3 that were studied – the small yellow bar is present to indicate that it was measured. Subsequently lactate is noted to increase

with tumor growth subsequently. At very large tumor volumes, the concentration of lactate is noted to decrease presumably due to necrosis. Histopathological analyses of tumors at different

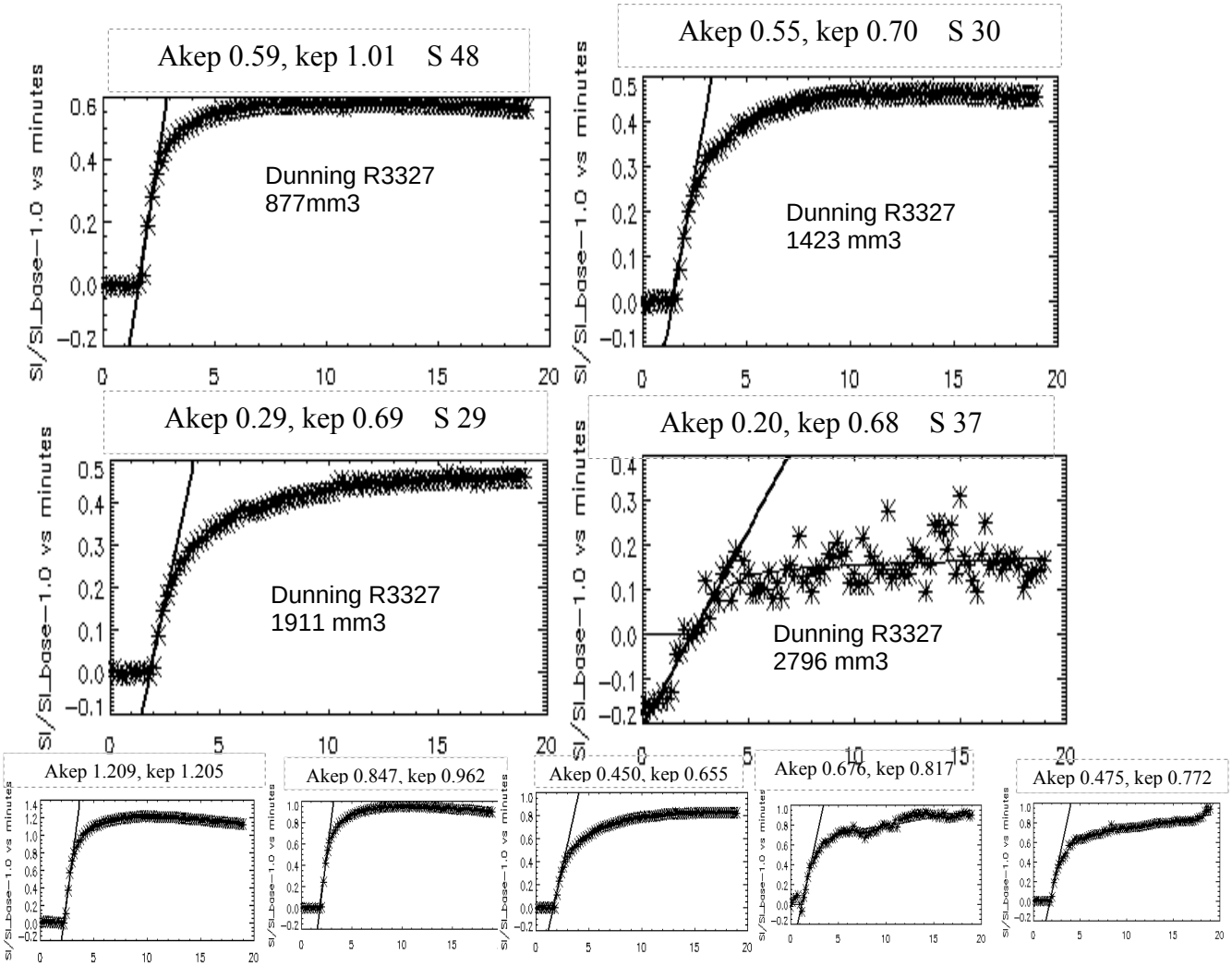

Fig. 5 Representative plots of percent increase in signal intensity vs. time (seconds) for the same animal as it grew from the volumes noted. Top: Dunning R3327AT. Bottom: Dunning H S=slope

sizes are pending. To estimate intra-tumor heterogeneity of lactate, the variation within a tumor was estimated by calculating the average lactate concentration in each voxel that was completely filled with tumor, and the standard error of the mean for each tumor. The values of the different standard errors of the mean for each study were then averaged for all the tumors and plotted in Figure 4 as a function of tumor volume. It is noted that the variation in lactate in each voxel based on the increase in the standard error of the mean increases with size except for very large tumors wherein they decreased. The tumor heterogeneity with respect to metabolism as manifested by variation in lactate concentration in a particular tumor, increases and decreases in a manner similar to the average concentration of lactate, ie when lactate is low there is little heterogeneity while when lactate concentration increases, there is increased heterogeneity. This suggests that at larger tumor volume, one would expect to see more histologic evidence of

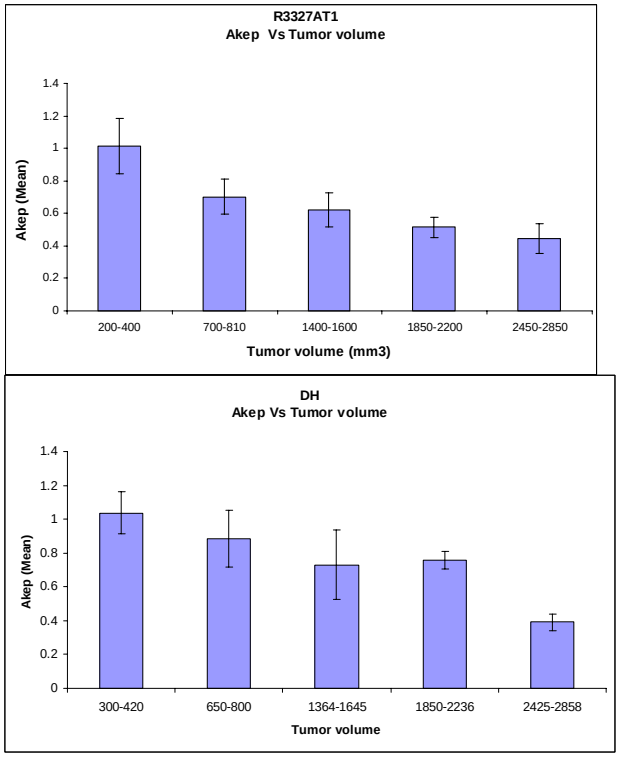

Fig. 6. Plots of average values of Akep for the R3327AT (top) and Dunning H (bottom) vs. tumor size. Behavior of both tumor models is similar.

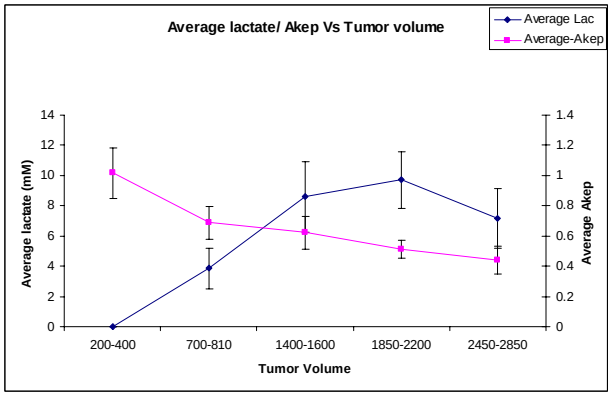

Fig. 7. Summary plot of changes in lactate and Akep with tumor volume.

variability in vasculature and necrosis and possibly hypoxia. These histopathologic evaluations are pending.

To determine the effect of growth on tumor perfusion and permeability, we performed dynamic contrast enhanced MRI studies immediately after acquisition of the lactate data. Figure 5 (top) shows a typical study from the Dunning R3327 at small tumor volume(877 mm3) and in the same animal at progressively larger tumor volumes. The slope and Akep decrease after the initial study at the smallest tumor. The data are relatively similar for both tumor models as noted in Fig. 6. The data from the different tumors acquired at different volumes are summarized in a bar graph in Fig. 6. Both the Dunning H and the R3327AT tumors show a decrease in Akep and the rate of increase of signal post injection of Gd-DTPA with tumor growth. Currently we are evaluating the data on a pixel by pixel basis to provide a histogram display to determine whether these results might be more informative. Fig. 7 is a summary plot of Akep and lactate concentration vs. tumor volume.

Data Presentation: Technical

Lactate is an important metabolite which reflects elevated tumor glycolysis and poor tissue perfusion, both of which are related to tumor development. The detection of lactate in tissues is difficult due to the presence of high concentrations of co-resonant lipid signals. In the accompanying work (above) using the SelMQC (5) method, varying lactate signal intensities were observed in rodent prostate R3337 tumors with increasing volumes. Here we report a novel modification of the SelMQC sequence using binomial spectral-selective pulses (SS-SelMQC) (Fig.8). Frequency selective excitation pulses were employed with suitable phase cycling of a binomial sequence $\left[(\pi/4)_{\phi 1} - \Delta - (\pi/4)_{\phi 2}\right]$ to selectively excite either lactate methyl CH_3 resonances (ϕ_1, ϕ_2=x, -x) or methylene CH

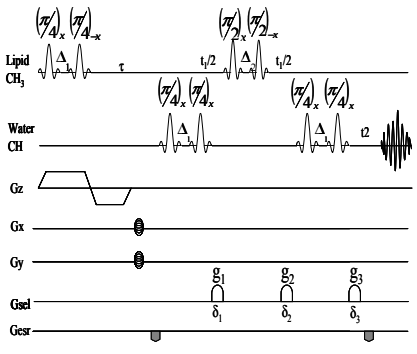

Fig.8 The SS-SelMQC pulse sequence; The ZQ →DQ coherence transfer path way is selected with the G_{sel} gradients in a ratio of 0:-1:2. τ=72 ms and MQ evolution period t_1= 26ms.

resonances (ϕ_1, ϕ_2=x, x). Frequency selective inversion was achieved using $[(\pi/2)_x - \Delta - (\pi/2)_{-x}]$ for the lactate methyl CH_3 resonances. Chemical shift selection was achieved by adjusting the interpulse delay equal to the inverse of twice the difference in the center frequencies of maximum and null excitation bands (Fig. 9). In a lipid enriched environment, the modified pulse sequence yielded enhanced lactate signal of 200-300% compared to SelMQC. Non-localized proton spectra and 2D CSI-lactate images were obtained from 30mM lactate/lipid phantoms and *in-vivo* R3327 prostate animal tumors.

NUMERICAL SIMULATIONS AND EXPERIMENTAL METHODS**:** Performance of the selective pulses were evaluated using computer simulations of these pulse blocks using AX spin system representing lactate (A=CH3; X=CH). Numerical simulations were generated using spin density matrix calculations. Selective excitation profile of binomial spectral-selective pulse is shown for CH3 (-560Hz) without disturbing CH (0 Hz) resonance (Fig.9a) and vice versa (Fig. 2b). The numerical simulations were carried out using MATLAB signal processing package.

All experiments were performed on a 4.7 Tesla Bruker Biospin spectrometer (40 cm horizontal bore). Animal studies were conducted in compliance with protocols approved by the animal care protocols in Memorial Sloan-Kettering Cancer Center. The rat was anesthetized using a mixture of isoflurane and air (20% O_2) and placed in the animal holder. The tumor was placed inside a 2 turn home built coil (25mm diameter) tuned and matched at 200MHz and MR experiments were initiated. The tumor volume was 857mm3 (using vernier calipers). The modified pulse sequence was tested using phantoms (cylinder 30mM lactate doped with 25uM Gd-DPTA/Crisco Fat), and demonstrated in vivo using a R3327-AT prostate tumor subcutaneously implanted on the thigh of a Copenhagen rat. MR spectroscopy acquisition parameters for SelMQC were taken from ref (5). In SS-SelMQC , we used high power three-lobe sinc shaped RF pulses for both 45° (200 us duration) and 90° (400us duration) flip angles, a pulse repetition of 2 s and spectral width of 12.5 ppm; Δ_1=693us; Δ_2=493us; Although we can use hard RF pulses, we used shaped pulses for low RF power dissipation and slice selection. Due to finite pulse widths, the interpulse delay was calculated by taking them into consideration. Transmitter was set at the CH frequency. Non-localized spectra were obtained with 16 transients. The 2D ^{1}H CSI was performed with a voxel size of 2.5×2.5x5 mm^3 (FOV=4.0cm). Total time for 2D CSI experiment was ~1 hr 15 minutes (ns=8). The ^{1}H-MRS images were reconstructed using 3DiCSI processing software. The intensity of each CSI voxel is proportional to the corresponding lactate spectral intensity. The anatomical T2 -^{1}H reference images were acquired using the same setup with a multiple spin-echo sequence.

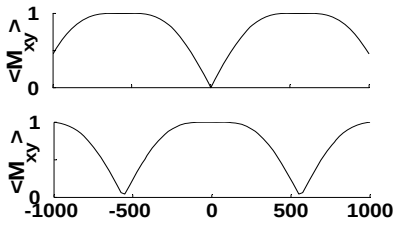

Fig.9 Theoretical excitation profile as a function of resonance frequency employing $\left[(\pi/4)_{\phi 1} - \Delta - (\pi/4)_{\phi 2}\right]$ with (ϕ_1, ϕ_2=x, -x) (a) and (ϕ_1, ϕ_2=x, x)(b)

RESULTS AND DISCUSSION: Fig 10 shows the non-localized spectra obtained from the phantom (MR image shown in (Fig.10a)) using SS-SelMQC showing lactate signal with complete suppression of lipid and water (Fig. 10b). Integrated lactate signal area is 3 times stronger than the signal obtained using SelMQC with same amount of water suppression level (Fig.10c). The same effect was demonstrated using R3337 tumor (Fig. 11). From this summed spectrum, the lactate signal to noise with SS-SelMQC is more than 200% that obtained with the

SelMQC. Experimental 16 x 16 2D-CSI lactate maps (Fig.12) were obtained from a 5 mm sagittal slice in the tumor region which was coregistered with a T2-weighted image. Varying amounts of lactate signal were present at different positions within the tumor In *in-vivo* situations with shorter T2 relaxation times, enhancement of signal to noise would be critical for accurate measurements and for absolute quantification of tissue lactate concentrations. This effect will be dominant in studies with small tumor volumes, where lactate concentrations may be low.

CONCLUSION: Lactate signals detected by SS-SelMQC have a 2-3 times higher signal to noise compared to conventional SelMQC. The sequence is currently being implemented for lactate detection from volume of interest, which will be used to image the internal organs of transgenic animal tumor models.

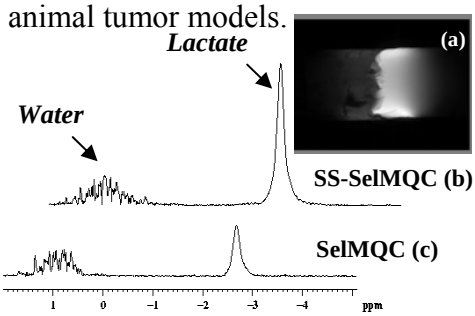

Fig10 Experimental non-localized ^{1}H spectra obtained from lactate/lipid phantom (MR image shown in (a)), using SS-SelMQC (b) and SelMQC (c). Note excellent lipid and water suppression

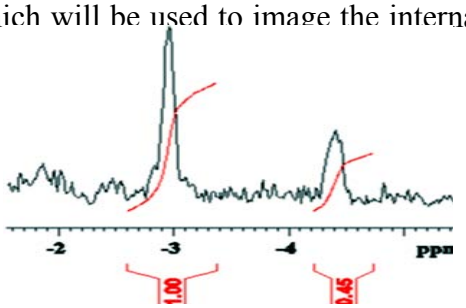

Fig.11.Sum of non-localized ^{1}H lactate spectrum o from SS-SelMQC and SelMQC. In SelMQC, lactate fre is shifted to -4.4ppm before adding to SS-SelMQC Integrated areas are labeled in red

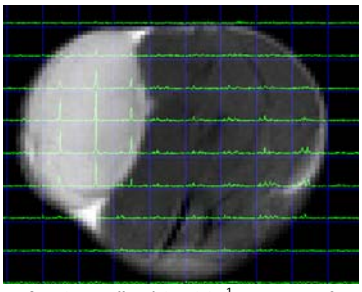

Fig.12 Localized 2D CSI ^{1}H spectra of lactate using SS-SelMQC

KEY RESEARCH ACCOMPLISHMENTS:

1. Differences between slow and fast growing tumors in lactate concentration measured.
2. Development of new, quantitative and more sensitive pulse sequence for lactate measurements implemented.

REPORTABLE OUTCOMES:

Two abstracts submitted for upcoming International Society of Magnetic Resonance in Medicine meeting. Both are in the process of being written for submission

1. Comparative study of tumor lactate and tumor vasculature in aggressive and indolent prostate cancer animal models by 2D-MR Spectroscopic Imaging and DCE-MRI – Yaligar et al

2. In-Vivo Lactate Detection Using Selective MQ Coherence Spectroscpy: Signal Enhancement Using Spectral-Selective Binomial RF pulses (SS-SelMQC) - Thakur et al

CONCLUSION: We have shown that lactate concentrations are present in a variable amount in a very aggressive tumor model (R3327AT) which is known to be radiation resistant. At small tumor volumes, lactate where greater radiation sensitivity is expected, lactate was not detected. Conversely, in a radiation sensitive tumor model (Dunning H), lactate cannot be detected. We have developed a modification to the pulse sequence for detecting lactate which is more sensitive and hope to apply it in future experiments. The use of DCE-MRI did not show suggest differences between the radiation resistant and radiation sensitive tumor model.

Future Plans

We are in the process of growing the Dunning HI and MATLyLu to compare metastatic and fast growing tumors and also compare with the data presented above. We will also compare the lactate measurements with a PET tracer of hypoxia (18F-fluoromisonidazole) to determine if lactate could be considered as a surrogate of hypoxia. The resolution of the lactate study will be improved to that of the PET study (~2 x 2 x 2 mm).

Another obstacle that we have encountered is that Roche has been reluctant to supply the anti-angiogenic agent that had been agreed upon. This is still being negotiated and we seem to have made progress last week.

REFERENCES:

1. Hoffman U, Brix G, Knopp MV et al. Pharmacokinetic mapping of the breast: A new method for dynamic MR mammography. Magn Reson Med33:506-514, 1995

2. Tofts PS, Kermode AG Measurement of the blood-brain barrier permeability and leakage space using dynamic MR imaging. 1. Fundamental concepts. Magn Reson Med. 1991 Feb;17(2):357-67.

3. Wang Y, Huang W, Panicek DM, Schwartz LH, Koutcher JA. Effects of Arterial Input Function Determination on Pharmacokinetic Modeling of Osteosarcoma Dynamic Contrast-Enhanced MRI Data. Magnetic Resonance in Medicine. In Press

4. Vanhamme L, van den Boogart A, Van Huffel S. Improved method for accurate and efficient quantification of MRS data with use of prior knowledge. J Magn Res 129: 35-43, 1997

5. He Q, Shungu DC, van Zijl PC, Bhujwalla ZM, Glickson JD. Single-scan in vivo lactate editing with complete lipid and water suppression by selective multiple-quantum-coherence transfer (Sel-MQC) with application to tumors. J Magn Reson B. 1995 Mar;106(3):203-11

APPENDICES: None